Finite Element Analysis of Rock Deformation in Deep Twin Tunnels

Felipe P. M. Quevedo[1], Carlos A. M. M. Colombo[1], Bianca M. Girardi[1], Denise Bernaud[1], Samir Maghous[1]

[1]*Federal University of Rio Grande do Sul*
Av. Osvaldo Aranha, 99, Porto Alegre, 90.035-190, RS, Brazil
motta.quevedo@ufrgs.br, ca-colombo@hotmail.com, eng.biancagirardi@gmail.com
denise.bernaud@ufrgs.br, samir.maghous@ufrgs.br

Abstract. Relying upon a three-dimensional finite element analysis, this contribution investigates the instantaneous irreversivel response induced by the constitutive behavior of the rock mass in the convergence profile of twin tunnels. At the rock material level, elastoplastic state equations based on a Drucker-Prager yield surface with an associated flow rule are adopted in the modeling. As regards the tunnel support, the formulation accounts for the presence of an elastic shotcrete-like lining. From a computational point of view, the deactivation-activation method is used to simulate the excavation process and the installation of the lining. The accuracy of the finite element predictions is assessed through comparisons with the available analytical solutions formulated in a simplified scenario for the twin tunnel configuration. A parametric study investigates the mutual interaction induced by the proximity of the tunnels.

Keywords: Twin tunnels, Elastoplasticity, Finite element modeling

1 Introduction

Many design methods often focus on single tunnels, but twin tunnels are a common occurrence. The interaction between tunnels can be significant, especially when the spacing between them is minimal. Additionally, many twin tunnels incorporate transverse galleries, introducing a localized effect on displacements and stresses. While the simulation of tunnel convergence in single tunnels has been widely investigated and reported in published literature, few works have addressed the computational evaluation of deformation in twin tunnels. Some studies on deep twin tunnels can be found at Spyridis and Bergmeister [1], Chen et al. [2], Ma et al. [3], Fortsakis et al. [4], Chortis and Kavvadas [5], Chortis and Kavvadas [6], Guo et al. [7], Chortis and Kavvadas [8], Chortis and Kavvadas [9]. But less attention has been dedicated to assessing the mutual mechanical interaction induced by the excavation of the transverse gallery connecting the twin tunnels.

In this context, the main contributions of this paper can be summarized at both the material and tunnel analysis levels. At the material level, the constitutive state equations of the rock mass are developed using a plasticity framework, which is suitable for clayey rocks. For the mechanical behavior of the concrete lining, the traditional linear elastic model are employed. At the structural analysis level, the deformation of the highly interactive components of the material system (i.e., rock mass and lining) resulting from the excavation of twin tunnels and transverse gallery is simulated using three-dimensional finite element simulations. The excavation and lining placement processes are simulated through the activation/deactivation technique. The constitutive models for the rock mass and the associated numerical integration schemes, are implemented into the UPF/USERMAT customization tool [10] of the ANSYS standard software. This three-dimensional finite element analysis is specifically designed to address the interactions induced by the construction process, the proximity of twin tunnels, and the presence of the transverse gallery.

2 Constitutive Models

The constitutive model for the rock mass corresponds to the associated Drucker-Prager elastoplastic model. The local strain rate $\dot{\varepsilon}$ is split into two contributions $\dot{\varepsilon} = \dot{\varepsilon}^e + \dot{\varepsilon}^p$, so that the constitutive relationships relating the Cauchy stress rate $\dot{\sigma}$ and strain rate components can be written as:

$$\dot{\sigma} = D : \dot{\varepsilon}^e = D : (\dot{\varepsilon} - \dot{\varepsilon}^p). \tag{1}$$

In the above relationship, $\dot{\varepsilon}^e$ and $\dot{\varepsilon}^p$, represent respectively the elastic and plastic strain rate, and D denote the fourth-order isotropic elastic linear constitutive tensor defined by the rock mass elastic Young modulus E and Poisson ratio ν. The plastic strain rate is given by flow rule:

$$\dot{\varepsilon^p} = \begin{cases} \dot{\lambda}\dfrac{\partial g}{\partial \sigma} & \text{for } f > 0 \\ 0, & \text{for } f \leq 0 \end{cases}, \tag{2}$$

where $\dot{\lambda}$ is the plasticity multiplier (obtained through the consistency condition $\dot{f} = 0$) and g is a potential flow function analogous to f used to simulate the volume dilatation during the evolution of plastic deformations. However, for this analysis, was used associated plasticity, i.e., $g = f$. In this model the Drucker-Prager plastic flow surface is given by

$$f(\sigma, q) = f(I_1, J_2, q) = \beta_1 I_1 + \beta_2 \sqrt{J_2} - q(\alpha), \tag{3}$$

which I_1 is the first invariant of the stress tensor, J_2 the second invariant of the deviator tensor and β_1, β_2 and $q(\alpha)$ are strength parameters related to the friction angle ϕ and cohesion $c(\alpha)$, respectively. In the present model Drucker-Prager surface been inner of the Mohr-Coulomb surface [16], that is,

$$\beta_1 = \frac{(k-1)}{3}, \quad \beta_2 = \frac{(2k+1)}{\sqrt{3}}, \quad q(\alpha) = 2\sqrt{k}\, c(\alpha), \tag{4}$$

where $k = (1+\sin\phi)/(1-\sin\phi)$. The internal variable α is the equivalent plastic strain $\bar{\varepsilon}^p$ used to simulate strain hardening/softening phenomena. However, for this study, we adopt perfect plasticity, meaning that c is a constant.

A linear elastic constitutive model is used for the concrete lining, which can be expressed, within the framework of infinitesimal analysis, as:

$$\dot{\sigma} = D : \dot{\varepsilon}^e, \tag{5}$$

where, $\dot{\varepsilon}^e$ and D are respectively the elastic strain rate and the fourth-order isotrpoic elastic constitutive tensor defined by the concrete lining Poisson ratio $\nu_c = 0.2$ and elastic Young modulus E_c.

3 Spatial and time discretization of the domain

The geometry material domain Ω considered for the finite element simulations, including tunnelling and deformation analysis, is defined by a parallelepiped volume of dimensions $(L_1 + L_2) \times L_3 \times d_3$ (Fig. 1). Owing to the symmetry of the problem, only the material portion $\{x \leq 0, y \geq 0\}$ is considered for F.E discretization and analysis. Referring to the notations of Fig. 1, d_1 is the distance between the axes of longitudinal tunnels, L_2 represents the total length along longitudinal direction e_z of the cylindrical volume to be excavated that is considered in the numerical simulation, d_3 is the thickness along vertical direction e_y of material domain Ω, L_1 stands for the length of unexcavated region after total excavation process, L_3 is the total length along transversal direction e_x of discretized material domain, d_2 characterizes the location of the circular transverse axis gallery that intersects the longitudinal tunnel at $z = L_1 + d_2$. The length of the excavation step adopted will be denoted by L_{pt}. The mesh used in the simulations consists of 119740 or 221104 total elements (hexahedra and tetrahedra), depending on the value of spacing between longitudinal tunnels. To increase the accuracy of the model predictions in the intersection zone, the region surrounding the transverse gallery (including part of the longitudinal tunnel) is discretized by means 10-node quadratic tetrahedral elements, whereas 8-node trilinear hexahedral elements are used for the remaining part of the structure. Furthermore, a refined meshing is used for discretizing the zones surrounding the longitudinal and transverse gallery. These zones whose mechanical state is significantly affected by the tunnelling process are indicated by light gray color in Fig. 1. Two values shall be considered for the spacing d_1 in the numerical simulations, namely $d_1 = 16R_t$ and $4R_t$. The layer of concrete lining of thickness e_g installed along the gallery wall is indicated by red color in the figure. Without introducing additional modeling restriction and for the sake of simplicity, the value of the gallery radius is fixed to $R_g = 2/3R_t$. The same lining system (same concrete material and layer thickness) is considered for both longitudinal tunnels and gallery. As regards the discretization of the region surrounding the gallery, parameters d_5 and d_1 define the size in a yz plane of the transition region involving the tetrahedral finite elements.

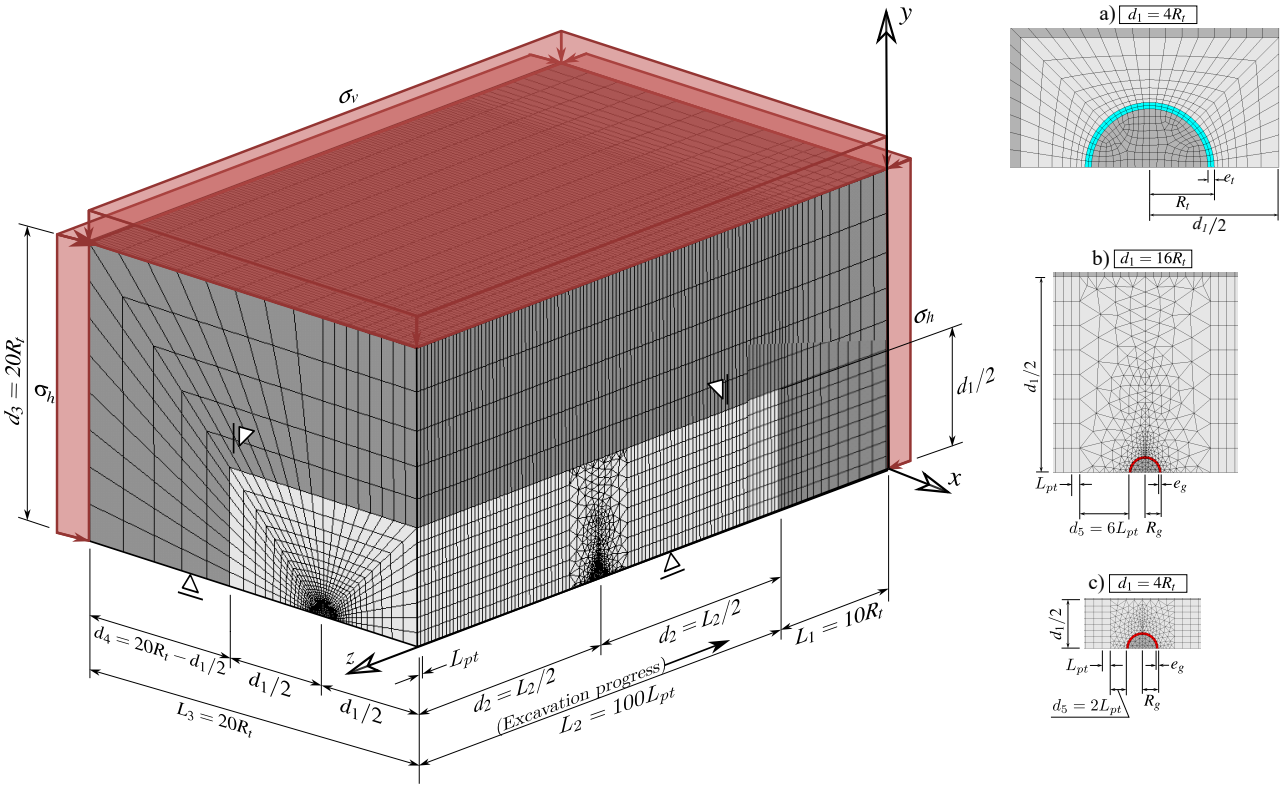

Figure 1. Geometry, mesh and boundary conditions of domain and details of a) longitudinal tunnel cross-section for configuration $d_1 = 4R_t$ and gallery cross-section for configuratoins b) $d_1 = 16R_t$ and c) $d_1 = 4R_t$.

As mentioned previously, the tunnelling process, including the excavation steps and lining installation, is simulated resorting to the activation-deactivation method shown in the schematic representation in Fig. 2. Each excavation step is modeled by deactivation of the corresponding elements (the elements stiffness is reduced by a factor $1E8$), whereas installation of elements of lining at a distance d_{0t} from the excavation face (unlined length) is achieved through activation of the corresponding elements by assigning them concrete properties. In this Figure, n_p is the total number of excavation steps and n_{pig} represents the number of longitudinal tunnel excavation steps prior to gallery excavation. After achievement of the n_{pig} excavation steps, the excavation of the gallery is initiated starting from the longitudinal tunnel wall. Referring to the notation of Fig. 2, L_{pg} is the considered step length for the gallery excavation, V_{pg} is the speed of the gallery excavation, and d_{0g} is the unlined length of the gallery. Each gallery excavation step is associated with pseudotime interval $t_{pg} = V_{pg}/L_{pg}$. After the gallery excavation is completed, we proceed to further excavation steps of the longitudinal tunnel. The main parameters defining the geometry domain as well as and excavation process and lining installation are summarized in Table 1.

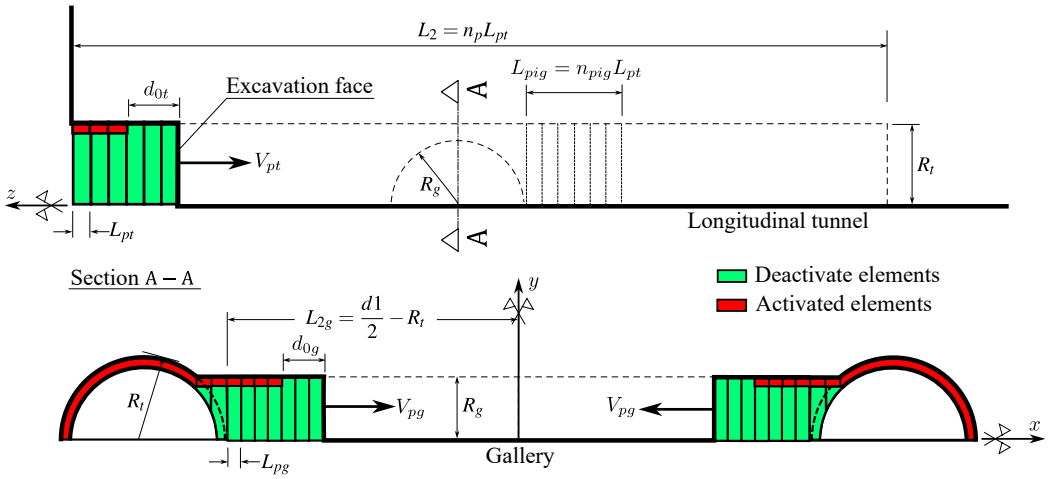

Figure 2. Schematic representation of the excavation process.

Table 1. Parameters related to the geometry of the domain, excavation and installation of the lining.

PARAMETERS	SYMBOL	UNIT	VALUES
Longitudinal tunnels			
Radius of the longitudinal tunnel	R_t	m	R_t
Thickness of the lining	e_t	m	$0.1R_t$
Step length of the excavation process	L_{pt}	m	$1/3R_t$
Unlined length	d_{0t}	m	$2L_{pt}$
Speed of the excavation face	V_{pt}	m/day	12.5
Excavation step time	t_p	day	L_{pt}/V_{pt}
Gallery			
Radius of the gallery	R_g	m	$2/3R_t$
Thickness of the concrete lining	e_g	m	$0.1R_t$
Step length of the excavation process	L_{pg}	m	$1/3R_g$
Unlined length	d_{0g}	m	$2L_{pg}$
Speed of the excavation face	V_{pg}	m/day	12.5
Number of steps that starts gallery excavation	n_{pig}	un	15
Rest of domain			
Distance between longitudinal tunnel axes	d_1	m	$4R_t$, $16R_t$
Length of the unexcavated region	L_1	m	$10R_t$
Total excavated length	L_2	m	$100L_{pt}$
Domain height	L_3	m	$20R_t$

4 Verification with unlined twin tunnel in elastoplastic medium

In the context of plane strain conditions, Ma et al. [3] developed an approximate analytical solution for the stresses and the plastic zone boundary around deep twin circular tunnels excavated in a homogeneous elastoplastic medium. This solution does not assume necessarily equal initial stresses, and the initial stress along the tunnel axis is assumed as the middle stress, i.e., $\sigma_{zz} = (\sigma_v + \sigma_h)/2$. For the constitutive model, the authors considered perfectly plastic Mohr-Coulomb criterion with associated plastic flow rule. In this analytical solution, it is assumed that the plastic zones around each tunnel are isolated from each other and completely surround each tunnel.

Fig. 3 shows the comparison between the 3D F.E. Solution (from a far behind the excavation face) and the analytical solution for plastic zone boundary provided in [3]. For these analysis, $R_t = 1$ m, $d_1/2R_t = 2.5$, Young's modulus $E = 20$ GPa, Poisson's ratio $\nu = 0.3$ and, friction angle $\phi = 30°$. The boundary of the plastic zone agrees very well with the elements that have reached the plasticity criterion.

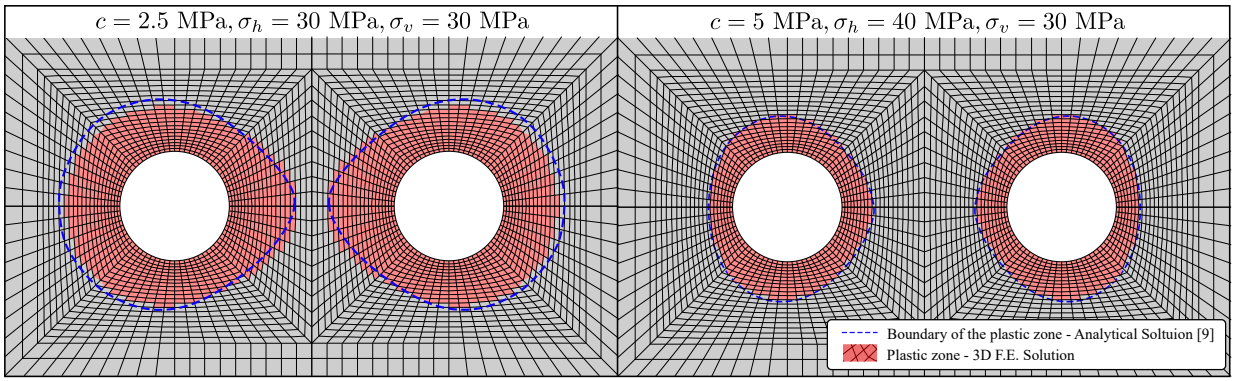

Figure 3. Comparisons between the numerical and analytical solution for the plastic zones considering $d_1/2R_t = 2.5$ and $\phi = 30°$ for different initial conditions and cohesion values.

.

The stresses obtained in the 3D numerical simulation are compared quantitatively in Fig. 4 with the stresses

derived from the elastoplastic analytical solution in [3]. This figure shows the radial and orthoradial stresses in polar coordinates (r, θ) considering three paths $\theta = 45°, 90°$ and $135°$. Although the criterion adopted for numerical simulation is the Drucker-Prager inscribed in Mohr-Coulomb, the solution agrees very well with the analytical solution in the plastic zone.

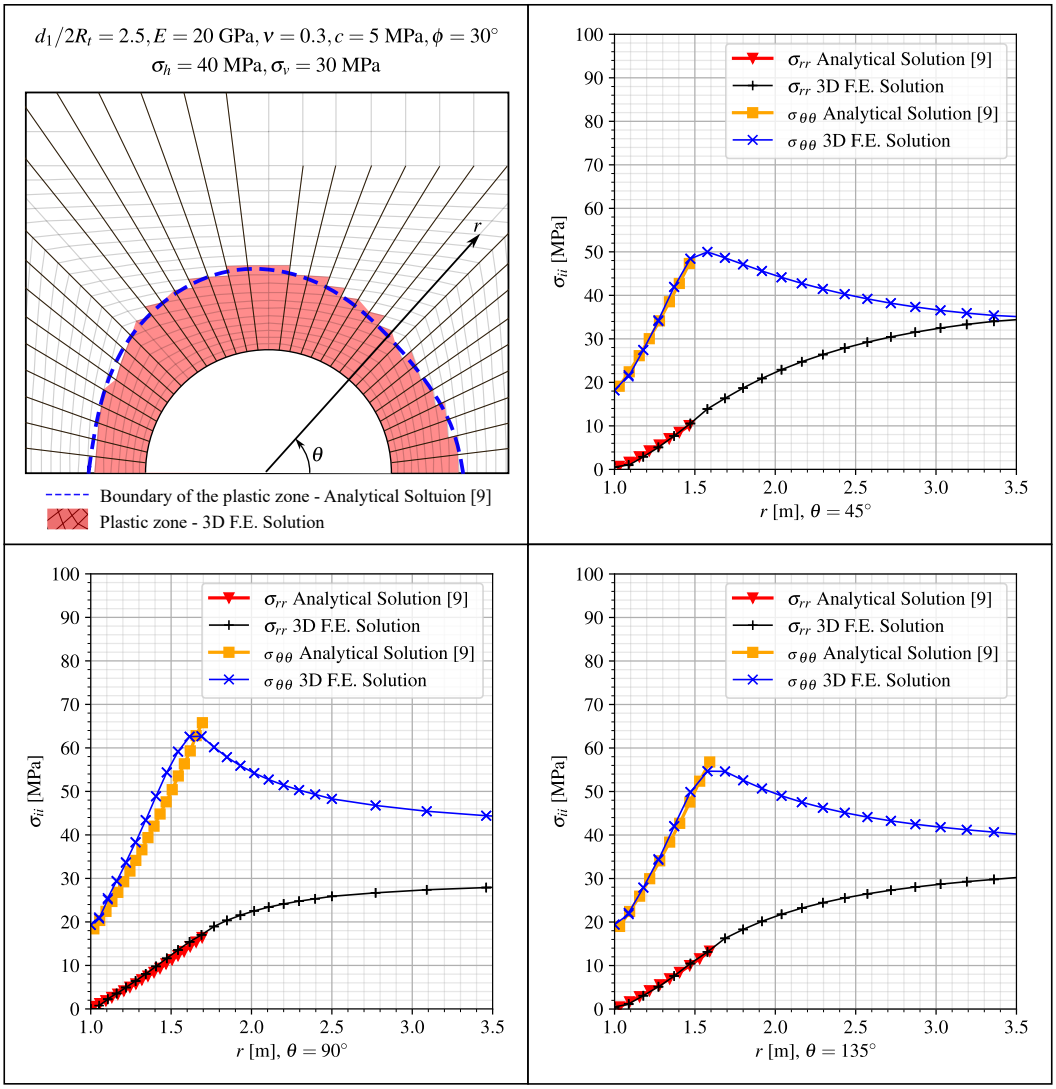

Figure 4. Comparisons between the numerical and analytical solution for differents stress-paths.

.

5 Numerical Results and Discussion

To study the effect of the lining, Fig. 5 and Fig. 6 show the elastoplastic rock mass (EP) under various conditions: without lining (NL), with a moderately stiff elastic lining ($K_c = 1027$ MPa), and with a highly stiff lining ($K_c = 3660$ MPa) with (WG) and without gallary (NG).

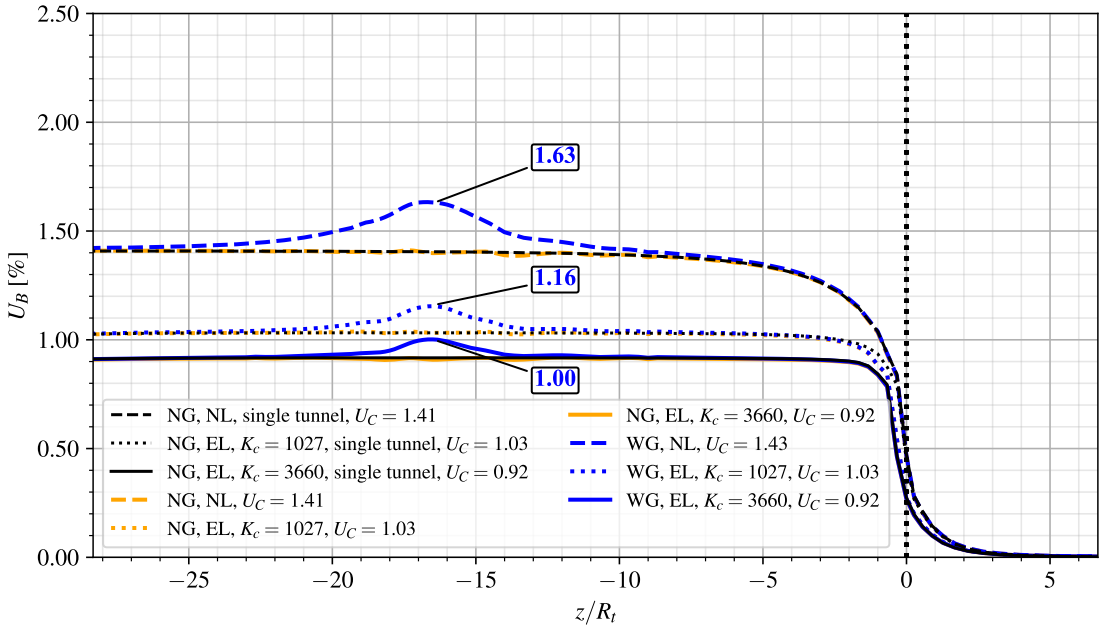

Figure 5. Convergence Profiles - elastoplastic rock mass (EP) without lining (NL) with a highly stiff elastic lining ($K_c = 3660$ MPa) and a moderately stiff elastic lining ($K_c = 1027$ MPa), without gallery (NG) and with gallery (WG) for $d_1 = 16R_t$.

.

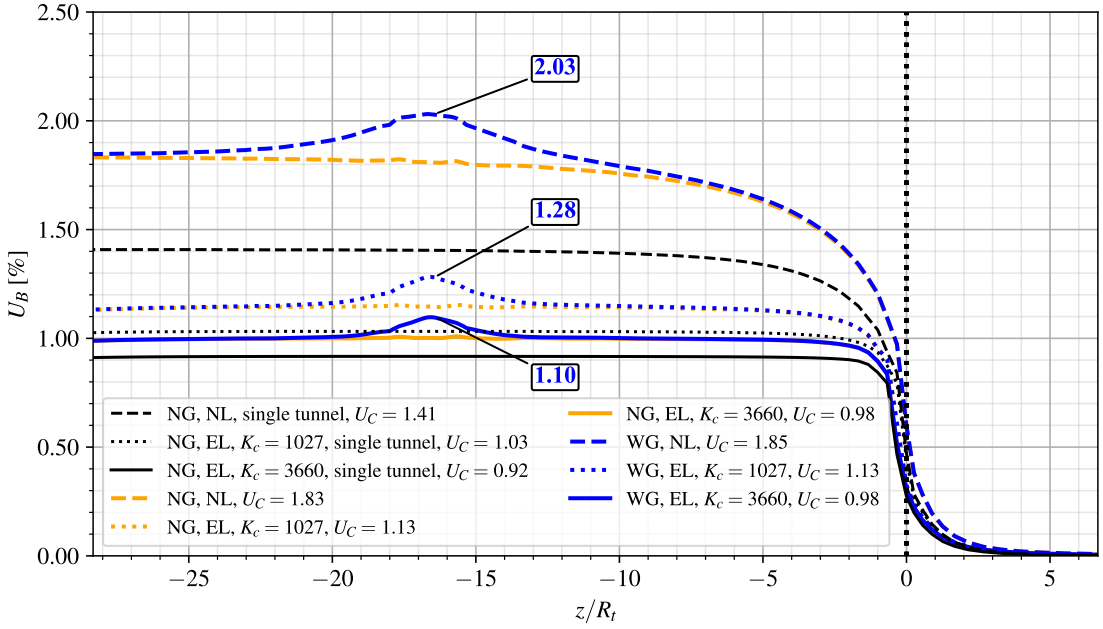

Figure 6. Convergence Profiles - elastoplastic rock mass (EP) without lining (NL) with a highly stiff elastic lining ($K_c = 3660$ MPa) and a moderately stiff elastic lining ($K_c = 1027$ MPa), without gallery (NG) and with gallery (WG) for $d_1 = 4R_t$.

.

For the single tunnel, a high stiffness lining (black solid line) decreases convergence by approximately 35% compared to the unlined model (black dashed line). Conversely, a moderately stiff lining (black dotted line)

increases convergence by 12% compared to the rigid lining.

When $d_1 = 16R_t$ between the twin tunnels (blue and yellow lines), the results of U_{eq} are similar to the isolated tunnel (black line). However, with a distance reduced to $d_1 = 4R_t$, the interaction between the tunnels becomes significant. A smaller d_1, the high stiffness lining (solid yellow and blue lines) can restrict convergence by up to 46% of the unlined (dashed yellow and blue lines) convergence. A moderate stiffness lining (dotted lines) leads to an increase of up to 16% in convergence compared to the high stiffness lining (solid lines).

When comparing results between twin lined tunnels with spacings of $16R_t$ and $4R_t$, differences of 6% with high stiffness lining (solid yellow and blue lines), 10% with moderate stiffness lining (dotted yellow and blue lines), and 30% without lining (dashed yellow and blue lines) are observed. These results show the direct impact of lining stiffness and the distance between twin tunnels on U_{eq} convergence.

When analyzing the convergence U_{peak} at the point where the gallery meets the longitudinal tunnel, there is an increase of 16% when using an moderate stiffness elastic lining (dotted blue line) compared to a high stiffness lining (solid blue line). However, when analyzing the difference between the U_{eq} and U_{peak}, there is a difference of up to 12% for the high stiffness elastic lining (solid blue line to $4R_t$ and $16R_t$) and up to 13% for the moderate stiffness elastic lining (dotted blue line to $4R_t$ and $16R_t$) for $d_1 = 4R_t$.

6 Conclusions

Type your conclusions or closing remarks here. Please be as concise and objective as possible. Do not make a summary of the paper, but instead list the main findings and results, even if these are only partial conclusions so far.

Acknowledgements. The authors are grateful for the financial support provided by CAPES and CNPq.

Authorship statement. The authors hereby confirm that they are the sole liable persons responsible for the authorship of this work, and that all material that has been herein included as part of the present paper is either the property (and authorship) of the authors, or has the permission of the owners to be included here.

References

[1] P. Spyridis and K. Bergmeister. Analysis of lateral openings in tunnel linings. *Tunnelling and Underground Space Technology*, vol. 50, pp. 376–395, 2015.

[2] F. Chen, L.-b. Lin, and D. Li. Analytic solutions for twin tunneling at great depth considering liner installation and mutual interaction between geomaterial and liners. *Applied Mathematical Modelling*, vol. 73, 2019.

[3] Y. Ma, A. Lu, X. Zeng, and H. Cai. Analytical solution for determining the plastic zones around twin circular tunnels excavated at great depth. *International Journal of Rock Mechanics and Mining Sciences*, vol. 136, pp. 104475, 2020.

[4] P. Fortsakis, E. Bekri, G. Prountzopoulos, and P. Marinos. Numerical analysis of twin tunnels interaction. In *Proc. 1st Eastern European Tunnelling Conference*, Budapest, Hungary, 2012.

[5] F. Chortis and M. Kavvadas. Three-dimensional numerical analyses of perpendicular tunnel intersections. *Geotechnical and Geological Engineering*, vol. 39, pp. 1771–1793, 2021a.

[6] F. Chortis and M. Kavvadas. Three-dimensional numerical investigation of the interaction between twin tunnels. *Geotechnical and Geological Engineering*, vol. 39, pp. 5559–5585, 2021b.

[7] Z. Guo, X. Liu, and Z. Zhu. An elastic solution for twin circular tunnels' stress in hydrostatic stress field. *Geotechnical and Geological Engineering*, vol. 39, pp. 1–11, 2021.

[8] F. Chortis and M. Kavvadas. 3D numerical investigation of the axial forces acting on tunnel junctions constructed in fractured/weathered to very blocky rockmass. In *Expanding Underground-Knowledge and Passion to Make a Positive Impact on the World*, pp. 1574–1582. CRC Press, 2023a.

[9] F. Chortis and M. Kavvadas. 3D numerical investigation of the bending moments acting on tunnel junctions constructed in fractured/weathered to very blocky rockmass. In *Expanding Underground-Knowledge and Passion to Make a Positive Impact on the World*, pp. 1583–1591. CRC Press, 2023b.

[10] ANSYS. *ANSYS Programmer's Reference, release 15.0*. Canonsburg, Pennsylvania, 2013.

[11] G. Rousset. *Comportement mecanique des argiles profondes: Application au stockage de déchets radioactifts*. Ph.D. Thesis (in french), Ecole Nationale des Ponts et Chaussées, Paris, France, 1988.

[12] D. Nguyen Minh and G. Rousset. Influence of instantaneous failure on time dependent behavior of underground galleries. In *The 28th U.S. Symposium on Rock Mechanics (USRMS)*, pp. ARMA–87–0663, Tucson, Arizona, 1987.

[13] A. Giraud and G. Rousset. Time-dependent behaviour of deep clays. *Engineering Geology*, vol. 41, n. 1, pp. 181–195, 1996.
[14] F. P. M. Quevedo, D. Bernaud, and S. Maghous. Numerical integration scheme for coupled elastoplastic–viscoplastic constitutive law for tunnels. *International Journal of Geomechanics*, vol. 22, n. 10, 2022.
[15] F. P. M. Quevedo. *Análise computacional das deformações em túneis profundos considerando o acoplamento plasticidade-viscoplasticidade*. Ph.D. Thesis (in portuguese), Federal University of Rio Grande do Sul, Porto Alegre, Brazil, 2021.
[16] D. Bernaud. *Tunnels profonds dans les milieux viscoplastiques: approches expérimentale et numérique*. Ph.D. Thesis (in french), Ecole Nationale des Ponts et Chaussées, Paris, France, 1991.
[17] P. Perzyna. Fundamental problems in viscoplasticity. In *Advances in applied mechanics*, volume 9, pp. 243–377. Elsevier, 1966.